Phys. Status Solidi B **252,** No. 10, 2215–2221 (2015) / **DOI** 10.1002/pssb.201552077

physica status solidi b
www.pss-b.com
basic solid state physics

Pressure-induced phase transition and dissociation of $PbMoO_4$

Shengxuan Huang[1], Xiaojing Lai[†,1], Feng Zhu[1], Xiang Wu[*,1], Ke Yang[2], and Shan Qin[,1]**

[1] Key Laboratory of Orogenic Belts and Crustal Evolution, MOE, Peking University and School of Earth and Space Sciences, Peking University, Beijing 100871, P.R. China
[2] Shanghai Synchrotron Radiation Facility, Shanghai Institute of Applied Physics, Chinese Academy of Sciences, Shanghai 201204, P.R. China

Received 9 February 2015, revised 28 May 2015, accepted 2 June 2015
Published online 7 July 2015

Keywords dissociation, $PbMoO_4$, pressure-induced phase transition, X-ray diffraction

* Corresponding authors: e-mail xiang.wu@pku.edu.cn, Phone/Fax: +86 10 62757892
** e-mail sqin@pku.edu.cn, Phone/Fax: +86 10 62751166
[†]Present address: Hawaii Institute of Geophysics and Planetology, University of Hawaii, Manoa

The high-pressure behavior of $PbMoO_4$ has been studied by *in situ* synchrotron radiation X-ray diffraction (XRD) combined with a diamond anvil cell (DAC) up to ~38 GPa. At room temperature, phase transitions of $PbMoO_4$ from the scheelite structure to the wolframite structure and then to amorphization are detected at ~8.3 and ~35 GPa, respectively. Pressure–volume relationships of $PbMoO_4$ are described by the Birch–Murnaghan equation of state, giving $V_0 = 355.8(3)$ Å^3, $K_0 = 73(4)$ GPa, $K_0' = 5(1)$ (third order) for the scheelite-structured phase and $V_0 = 166(1)$ Å^3, $K_0 = 85(4)$ GPa, $K_0' = 4$ (fixed) (second order) for the wolframite-structured phase. When $PbMoO_4$ undergoes the high-temperature annealing treatment at ~17.5 GPa, it will dissociate into assembly of the PbO (*Pbcm* and $Z = 4$) and $PbMo_2O_7$ ($P2_1/c$ and $Z = 4$).

1 Introduction ABO_4-type compounds, such as $PbMoO_4$, $CaWO_4$, $CrVO_4$, and $PbCrO_4$, have been extensively studied for a few decades because of their interesting structural properties and great potential in material science. For example, scheelite-structured ABO_4-type compounds are widely applied in scintillating materials [1–4], solid-state lasers [5], luminescence [6, 7], optoelectronic devices [8], and double-β decay experiments [9]. At ambient conditions, ABO_4-type compounds adopt various crystal structures attributed to different ionic radii and chemical valences of A-site and B-site cations. Metal molybdates and tungstates with large bivalent cations, such as Pb, Ba, and Eu, crystallize in the scheelite structure (space group: $I4_1/a$ and $Z = 4$), where each A-site cation is coordinated by eight O anions forming a AO_8 polyhedron and each B-site cation is coordinated by four equivalent O anions forming a BO_4 tetrahedron (Fig. 1a) [10–12]. On the contrary, those with relatively small A-site cations, such as Mn, Fe, and Mg, crystallize in the wolframite structure (space group: $P2/c$ and $Z = 2$), where the coordination number is 6 for both A-site and B-site cations (Fig. 1b) [13, 14]. By contrast, some other ABO_4-type compounds adopt zircon structure (space group: $I4_1/amd$ and $Z = 4$) [15] and monazite structure (space group: $P2_1/n$ and $Z = 4$) [16] at ambient conditions.

High pressure, as one important thermodynamic parameter, can strongly affect a material's structures and properties. Therefore, this fact has inspired a renewed interest in the fundamentally physical and chemical properties of ABO_4-type compounds. Diverse polymorphs of ABO_4-type compounds have been confirmed at high pressure in previous studies. A first-order phase transition to an unknown phase of $PbWO_4$ was observed at ~5.0 GPa by XRD [10]. $CaWO_4$, $SrWO_4$, and $SrMoO_4$ underwent the second-order phase transition from the scheelite structure to the fergusonite structure (space group: $C2/c$ and $Z = 4$) at ~11–13 GPa [17, 18]. $BaWO_4$ first has a scheelite-to-fergusonite phase transition at ~7.1 GPa and then undergoes a second transition to the $BaWO_4$-II-type structure (space group: $P2_1/n$ and $Z = 8$) at ~10.9 GPa [19]. The similar transition sequences were also detected in $PbWO_4$ at ~9 and ~15 GPa, respectively [19]. In addition, it was reported that some of the ABO_4 compounds became amorphous with increasing pressure, such as $BaWO_4$ at ~47 GPa [19] and $CaWO_4$ at ~40 GPa [20].

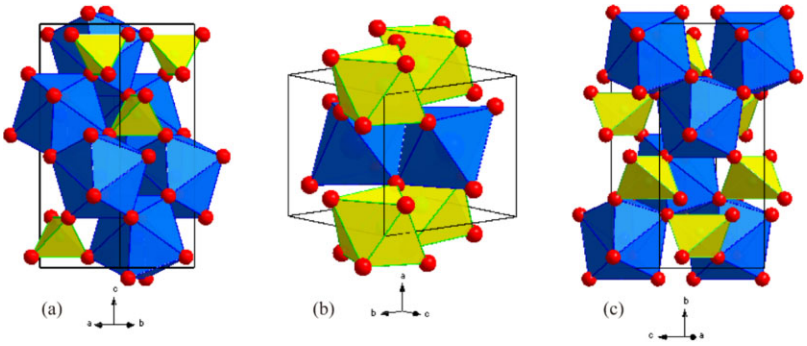

Figure 1 The scheelite ($I4_1/a$ and $Z=4$) (a), wolframite ($P2/c$ and $Z=2$) (b), and fergusonite ($C2/c$ and $Z=4$) (c) structures of ABO_4-type compounds. The blue and yellow objects represent the coordination polyhedra of A cation and B cation, respectively. Red solid circles represent the O anion.

Based on previous experimental and theoretical results, there is a general understanding of the pressure-induced phase transition sequences of ABO_4 compounds: zircon-type (or monazite-type) → scheelite-type → fergusonite-type (or wolframite-type) → $BaWO_4$-II-type → *Cmca* → amorphization [17–27]. In addition, the effect of temperature on structures is also complicated. In addition, the use of different pressure transmitting media in DAC experiments can cause different changes of structures. For example, the post-scheelite structure for ABO_4 compounds is always the fergusonite type under hydrostatic conditions while it tends to be the wolframite type under non-hydrostatic conditions, especially when no pressure transmitting medium is used [28, 29].

$PbMoO_4$ wulfenite, as a representative of ABO_4 compounds, has been reported to undergo a scheelite-to-fergusonite phase transition at ~10.6 GPa at room temperature, in which the coordination numbers of A-site and B-site cations remain unchanged (Fig. 1c) [30–32]. However, in the previous literature, there was not enough available information about the post-scheelite $PbMoO_4$, such as elasticity and stability. Therefore, in this study, we reinvestigated the behavior of $PbMoO_4$ in a higher range of both pressure and temperature in order to explore the elasticity and stability of $PbMoO_4$.

2 Experimental The natural wulfenite sample used in this study was a saffron yellow single crystal, collected from a lead–zinc deposit in Guizhou Province, P.R. China. The chemical composition of this natural mineral was checked by an emission scanning electron microscope (SEM) equipped with energy-dispersive spectroscopy (EDS) using INCA X-MAX50. There were only three elements Pb, Mo, and O in the sample obtained in the experiments and the ratio of Pb/Mo was 1:1.08 on average. These results implied that the chemical composition of the sample was consistent with the chemical formula $PbMoO_4$. The sample was ground into a fine powder for the experiments.

Four-pin-modified Merrill-Basset diamond anvil cells with diamond anvils of 300 μm in diameter were employed to produce the high pressure in two runs of experiments; 100–110 μm diameter holes were drilled in the preindented 30–40-μm rhenium gasket as the sample chambers. In run 1, silicone oil (CAS number 63148-62-9, Alfa Aesar) was used as pressure-transmitting medium and Au was utilized as internal pressure indicator [33, 34]. In run 2, the sample was sandwiched by LiF plates, which acted as both a pressure-transmitting and a thermal-insulating medium. The pressure was calibrated by the equation of state of LiF [35]. High-temperature annealing was employed at a certain pressure in run 2 by a portable laser heating system with 1064-nm laser radiation to overcome the potential kinetic effects on the phase transition and relax the stress gradient in the DAC [36].

Both runs of *in situ* high-pressure synchrotron X-ray powder diffraction experiments were carried out at beamline 15U of Shanghai Synchrotron Radiation Facility (SSRF), China. The focused monochromatic beams were selected with wavelength $\lambda = 0.6049$ Å and beam size $= 4 \times 3\ \mu m^2$ for run 1 and $\lambda = 0.6199$ Å and $3 \times 2.5\ \mu m^2$ for run 2. XRD patterns were recorded by a Rayonix SX165 CCD detector with an exposure time of 10–30 s. The conversion from Debye rings to one-dimensional X-ray profiles *versus* 2θ was done by the FIT2D software [37]. The XRD data were analyzed by the model-biased Le Bail fitting with GSAS + EXPGUI software [38].

3 Results In run 1, *in situ* high-pressure XRD patterns of $PbMoO_4$ were collected up to ~38 GPa at room temperature. Selected XRD patterns are presented in Fig. 2. The characteristic Bragg peaks of (101), (112), (004), and (200) helped to identify samples with the scheelite structure. The fitting results and structural parameters of scheelite-type $PbMoO_4$ are presented in Fig. 3a and Table 1, respectively. Upon compression, the diffraction peaks shifted generally to the higher 2θ angle. At ~8.3 GPa, there were new peaks appearing at 2θ of ~11.7° and ~14.3° (Fig. 2b). This indicated the occurrence of a pressure-induced phase transition. With increasing pressure, the (112) reflection split into two peaks, and the latter one shifted faster than the former one. We did not find any additional phase transition or decomposition up to ~38 GPa at room temperature. The Bragg peaks broadened upon compression possibly caused by a highly quasihydrostatic pressure environment [39, 40]. In particular, there was a bulge at 2θ of ~12° (Fig. 2f), which implied the amorphization of $PbMoO_4$. Additionally, the phase transition was reversible on decompression (Fig. 2g).

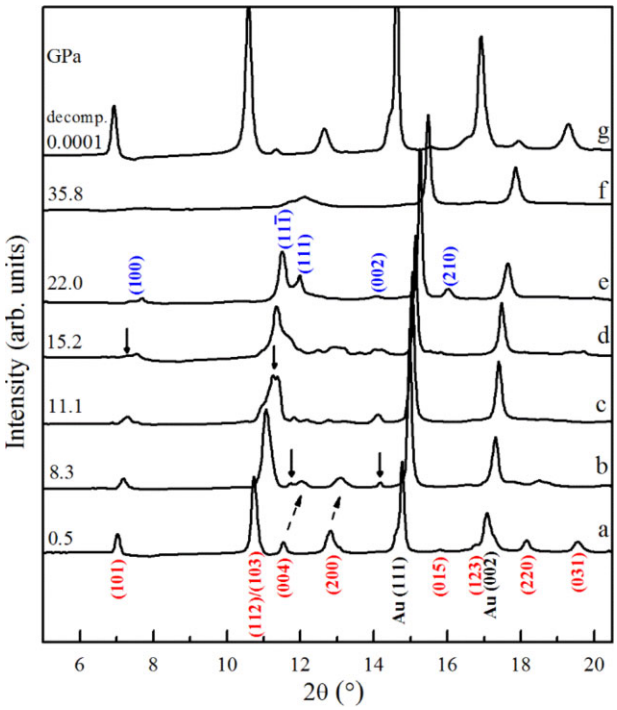

Figure 2 Selected ADXRD patterns of $PbMoO_4$ under different pressure conditions in run 1. The reflections of scheelite-type $PbMoO_4$, wolframite-type $PbMoO_4$, and Au are pointed out by the red, blue, and black numbers, respectively. The solid arrows represent the appearance of new Bragg reflections. The dashed arrows show the shift of Bragg reflections upon compression.

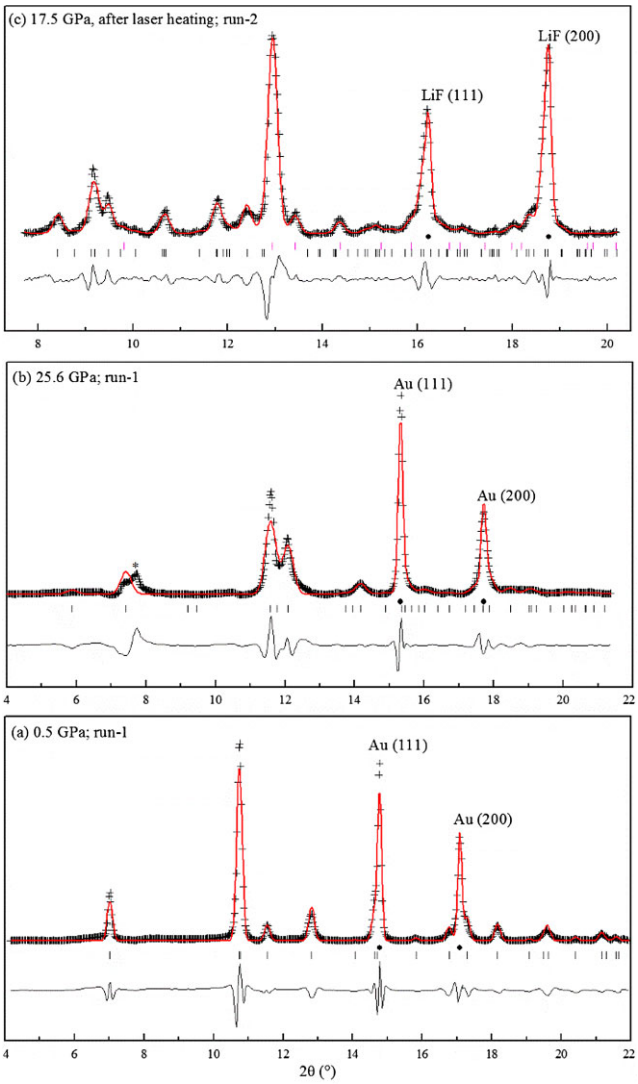

Figure 3 The fitting results of XRD patterns by the model-biased Le Bail method under different conditions. Backgrounds were subtracted from the original data. Measured (black crosses), calculated (red continuous line) intensities, positions of the reflections (black and pink short bars), and difference curve (black continuous line) between observed and calculated spectra are shown, respectively. Solid circles (•) represent peaks of the internal pressure indicators. The star (*) in (b) represents the peak that cannot be fitted. (a) 0.5 GPa, 300 K (run 1), (b) 25.6 GPa, 300 K (run 1), (c) 17.5 GPa, 300 K (run 2, after laser heating).

As presented above, the structure of $PbMoO_4$ changed at ~8.3 GPa according to the appearance of new Bragg peaks. The fergusonite-type structure, as the reported post-scheelite structure for $PbMoO_4$, was the first one to be taken into account. However, the tendency of changes for Bragg peaks did not match the fergusonite-type structure reported by other researchers [17–19, 31]. There are several reasons for this, as follows. First, the fergusonite-type structure cannot explain the appearance of the new peak at 2θ of ~11.7° at ~8.3 GPa (Fig. 2b). Secondly, the (200) reflection weakened gradually rather than split into two peaks after the transition. Thirdly, the characteristic (020) reflection for fergusonite-type structure could not be observed upon compression. Finally, the former of the two peaks split from the (112) reflection shifted to the higher 2θ angle rather than to the lower 2θ angle like fergusonite-type structure. In a word, the high-pressure phase of $PbMoO_4$ in this experiment could not be assigned to the fergusonite-type structure. We found that the patterns could be fitted by the wolframite-type structure though the (011) and (110) reflections were absent in the measured diffraction patterns (Fig. 3b and Table 1). In the meantime, the patterns could not fitted by the other structures mentioned in the Introduction section.

In run 2, the sample was laser heated to about 1,500 (±200) K at ~18 GPa for about half an hour and then quenched. The XRD pattern after high-temperature annealing (Fig. 4) was completely different from those in Fig. 2 at room temperature. In Fig. 4, the new diffraction peaks could be indexed to neither scheelite-type structure nor wolframite-type structure, which implied that these two phases were unstable under such conditions. In addition, the Bragg peaks only broadened upon compression caused by the quasihydrostatic status mentioned above [39, 40], which suggested that the new diffraction pattern was stable up to ~25.7 GPa.

Table 1 Structural parameters of scheelite-type $PbMoO_4$, wolframite-type $PbMoO_4$, $PbMo_2O_7$, and PbO at different conditions obtained in runs 1 and 2.

	run 1		run 2	
phase	scheelite-type $PbMoO_4$	wolframite-type $PbMoO_4$	$PbMo_2O_7$	PbO
space group	$I4_1/a$	$P2/c$	$P2_1/c$	$Pbcm$
p (GPa)	0.5	25.6	17.5	
a (Å)	5.419(1)	4.674(3)	7.537(3)	5.308(3)
b (Å)		5.901(6)	5.108(2)	4.958(3)
c (Å)	12.026(4)	4.908(3)	13.39(1)	4.219(2)
β (°)		93.24(3)	117.97(3)	
V(Å^3)	353.2(1)	135.2(1)	455.3(2)	111.04(5)
wRp	0.234	0.233	0.175	
Rp	0.182	0.166	0.124	

First, we could identify the pressure-transmitting medium LiF with strong intensities marked with black numbers in Fig. 4. According to the *ab initio* theoretical calculations, it has been investigated that either $BaWO_4$-II-type or *Cmca* structure has a lower enthalpy or energy than other phases considered for post-scheelite-type ABO_4 compounds in a higher pressure range and the failure of

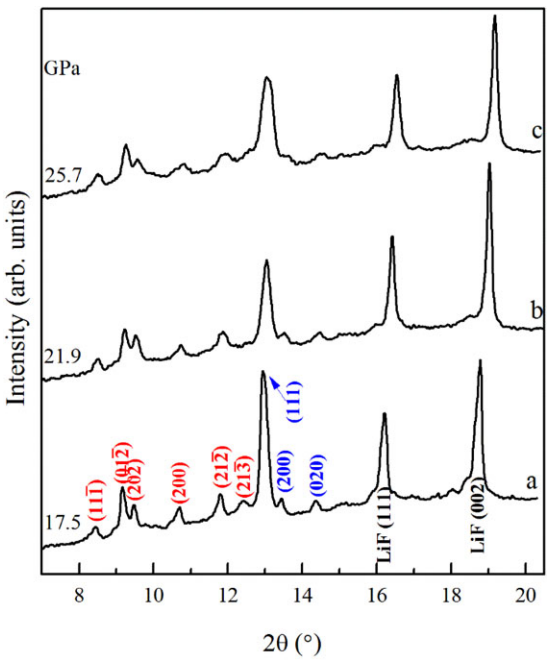

Figure 4 Selected ADXRD patterns of $PbMoO_4$ at different pressure conditions in run 2. Some representative reflections of $PbMo_2O_7$, PbO and LiF are pointed out by red, blue, and black numbers, respectively.

the phase transition results from the existence of kinetic barriers [17, 19, 41]. However, in our study, the peaks at 2θ of ~9.5°, ~10.7°, and ~14.35° (Fig. 4a) seemed to contradict those models. The remaining peaks could be divided into two groups. The peaks of the first group assembling between 7° and 13° shifted faster than those of the second group assembling between 13° and 15° (Fig. 4a). This behavior indicated that the sample dissociated into two compounds at extreme conditions. Our XRD data suggested that the second group belonged to the β-PbO phase (space group: *Pbcm* and $Z = 4$) [42]. We could rule out the possibility that the $PbMoO_4$ dissociated into a mixture of PbO and MoO_3, as proposed by previous work for the similar compound $SrWO_4$ [43]; in such a case, a phase transition from the monoclinic MoO_3-II phase (space group: $P2_1/m$) to the monoclinic MoO_3-III phase (space group: $P2_1/c$) should be observed upon compression [44]. However, the peaks of the first group could not be assigned to any polymorph of MoO_3, and the behavior of diffraction peaks on compression did not correspond to the expected MoO_3 structural changes. Therefore, the decomposition of $PbMoO_4$ into PbO and MoO_3 was not consistent with our experimental observations. Instead, we suggested that $PbMoO_4$ dissociated into a new assemblage with a possible chemical equation,

$$2PbMoO_4 \rightarrow PbO + PbMo_2O_7,$$

where the first group of diffraction peaks was assigned to the monoclinic $PbMo_2O_7$ phase (space group: $P2_1/c$ and $Z = 4$). Figure 3c presents the fitting results of the XRD pattern from a mixture of LiF (pressure marker and thermal insulator for laser heating), β-PbO, and $PbMo_2O_7$ at ~17.5 GPa. The structural parameters are shown in Table 1. The good statistical fit implied that the physical model was reasonable. However, the more details about the mechanism of decomposition for $PbMoO_4$ samples need confirmation using transmission electron microscopy and/or X-ray absorption spectroscopy [45, 46] in the future.

4 Discussion The compressions of lattice parameters for low- and high-pressure phases are shown in Fig. 5. For the scheelite structure, it presents the obvious fact that the compression of $PbMoO_4$ is highly anisotropic, i.e., the compressibility of the c-axis is larger than that of the a-axis. The axial compression coefficients are $\beta_a = -2.87 \times 10^{-3}$ GPa^{-1} and $\beta_c = -5.18 \times 10^{-3}$ GPa^{-1} by a linear fitting. And the ratio of c/a decreases from 2.219 to 2.186. This phenomenon that the c-axis is likely to be more compressible than the a-axis is related to the scheelite-type structure (Fig. 1a), where the much more rigid MoO_4 tetrahedra are directly aligned along the a-axis and each Pb cation locates between two MoO_4 tetrahedra along the c-axis forming a much softer PbO_8 polyhedron. The scheelite-to-wolframite phase transition is a little uncommon. It has been investigated that the scheelite-to-fergusonite phase transition can be detected under hydrostatic conditions and

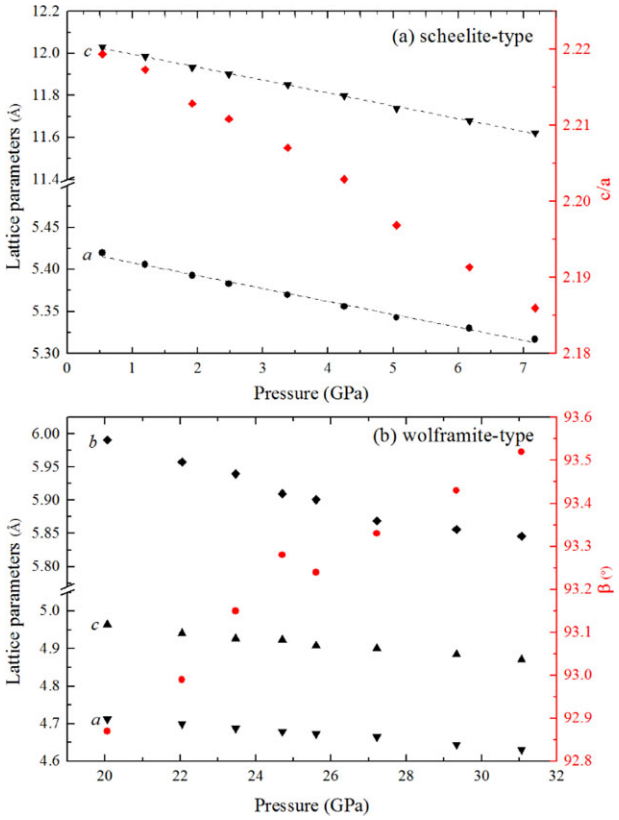

Figure 5 The experimental results of lattice parameters (a) a, c, and c/a of the scheelite-type $PbMoO_4$, and (b) a, b, c, and β of the wolframite-type $PbMoO_4$ as a function of pressure.

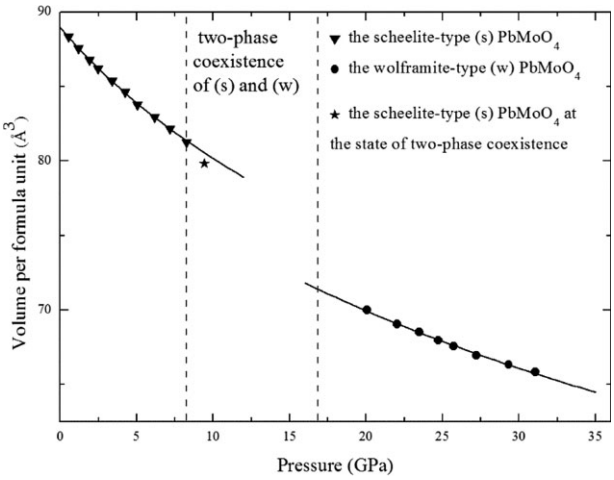

Figure 6 Experimental results of volume per formula unit as a function of pressure. Solid triangles, circles, and the asterisk represent the normalized volume of scheelite-type $PbMoO_4$, wolframite-type $PbMoO_4$, and scheelite-type $PbMoO_4$ at the state of two-phase coexistence, respectively. The solid line segments are calculated by the third-order (for scheelite-type $PbMoO_4$) and second-order (for wolframite-type $PbMoO_4$) Birch–Murnaghan equation of state. The region between the two dashed lines represents the state of two-phase coexistence.

the scheelite-to-wolframite phase transition is due to large deviatoric stresses [29]. In the previous studies, the 16:4:1 methanol–ethanol–water mixture [30] and the 4:1 methanol–ethanol mixture [31, 32] were used as the pressure-transmitting media, which could cause smaller deviatoric stresses than the silicone oil used in our experiments, at least below 12 GPa [40]. Additionally, two phases coexist between ~8.3 and ~17 GPa, which is typical of the scheelite-to-wolframite phase transition. Scheelite-type and wolframite-type structures have similar structures to some extent, both of which can be regarded as layer structures. According to Ref. [47], this is a reconstructive phase transition, whose mechanism is related to a shift of the Mo cation from the center of the MoO_4 tetrahedron towards the center of the MoO_6 octahedron, indicating an increase of coordination number for Mo cation. It is also commonly accepted that the atomic structures of ABO_4 compounds under high pressures are supposed to tend to structures with a higher and equal coordination of both A-site and B-site cations [47]. In our fitting, the ratio of $2c/a$ in wolframite-type structure is 2.107 at ~20 GPa. This result is approximately equal to the ratio of c/a in scheelite-type structure, which is in agreement with Errandonea's theory [47].

The compression of volume (Fig. 6) is fitted by the Birch–Murnaghan equation of state [48],

$$P(V) = \frac{3}{2}K_0\left[\left(\frac{V_0}{V}\right)^{\frac{7}{3}} - \left(\frac{V_0}{V}\right)^{\frac{5}{3}}\right]\left\{1 + \frac{3}{4}(K_0' - 4)\left[\left(\frac{V_0}{V}\right)^{\frac{2}{3}} - 1\right]\right\}$$

for both low-pressure and high-pressure phases. The results of zero-pressure volume (V_0), bulk modulus (K_0), and its first pressure derivative (K_0') for the low-pressure phase are summarized and compared with those of $PbMoO_4$ obtained by previous work in Table 2. The results are basically in good agreement with the previously reported data except the large first pressure derivative of bulk modulus in Ref. [30],

Table 2 The Birch–Murnaghan equation of states parameters of scheelite-type phase for different $PbMoO_4$ samples.

$PbMoO_4$ compounds	pressure range (GPa)	V_0 (Å^3)	K_0 (GPa)	K_0'	reference
natural samples	0–8.3	355.8(3)	73(4)	5(1)	this work
natural samples	0–10.6	362.5(6)	71(10)	29(3)	[30]
single crystal	0–6.0	357.6(3)	64(2)	4(fixed)	[10]
bulk crystalline	0–10.7	356.1(8)	67(4)	8(2)	[31]
nano-crystalline	0–16.1	355.9(8)	69(5)	6(2)	[31]

which is unusual and unphysical. In a word, the difference in the elasticity of scheelite-type phase is not significantly distinguishable for different $PbMoO_4$ samples. The results of fit to the high-pressure phase are $V_0 = 166(1)$ Å^3, $K_0 = 85(4)$ GPa, and $K_0' = 4$ (fixed). In addition, the calculating collapse of volume is ~6% at the transition, which indicates a first-order phase transition.

High-pressure (HP) and high-temperature (HT) experiments have been widely applied to investigate behavior of ABO_4 compounds as well. Lacomba-Perales *et al*. reported HP-HT *ex situ* and *in situ* experiments in $BaWO_4$ up to 7.5 GPa and 2,000 K [49, 50]. The scheelite-type structure was found stable up to 2,000 K at 2 GPa and metastable up to 6 GPa below 600 K. From their studies, we can determine that the stable structure of $BaWO_4$ is more sensitive to pressure than temperature. However, due to their small pressure range, it is hard to present a comprehensive view toward phase transition and stability of ABO_4 compounds. In addition, there is an unknown region in the phase diagram of $BaWO_4$ reported by Errandonea and Manjón [51]. In our study, we observed the dissociation of $PbMoO_4$ into PbO and $PbMo_2O_7$ under HP–HT conditions, which might provide a new view or clue for behavior of ABO_4 compounds under extreme conditions. Additionally, chemical changes of $PbMoO_4$ can lead to formation of complex compounds rather than only decomposition to simple oxides, which may help us comprehend migration of trace elements in the subduction zone or the lower mantle.

5 Conclusions The high-pressure elasticity and stability of $PbMoO_4$ have been investigated by ADXRD and DAC techniques up to 38 GPa. It has been found that the compression of scheelite-type $PbMoO_4$ with increasing pressure is anisotropic. The results reveal the reversible phase transition from the scheelite structure to the wolframite structure at ~8.3 GPa and to the amorphization at ~35 GPa at room temperature. The dissociation of $PbMoO_4$ into PbO and $PbMo_2O_7$ can be observed after being laser heated at high pressure. Finally, the pressure–volume relationship is fitted by the Birch–Murnaghan equation of state, which yields $V_0 = 355.8(3)$ Å^3, $K_0 = 73(4)$ GPa, $K_0' = 5(1)$ (third order) for low-pressure phase and $V_0 = 166(1)$ Å^3, $K_0 = 85(4)$ GPa, $K_0' = 4$ (fixed) (second order) for high-pressure phase of $PbMoO_4$.

Acknowledgments This work was supported by the Natural Science Foundation of China (41473056 and U1232204). The authors are grateful for the suggestions from the anonymous reviewer and the editor.

References

[1] M. Ishii and M. Kobayashi, Prog. Cryst. Growth Charact. Mater. **23**, 245 (1992).
[2] A. A. Annenkov, M. V. Korzhik, and P. Lecoq, Nucl. Instrum. Methods Phys. Res. A **490**, 30 (2002).
[3] M. Nikl, V. V. Laguta, and A. Vedda, Phys. Status Solidi B **245**, 1701 (2008).
[4] P. Lecoq, I. Dafinei, E. Auffray, M. Schneegans, M. V. Korzhik, O. V. Missevitch, V. B. Pavlenko, A. A. Fedorov, A. N. Annenkov, V. L. Kostylev, and V. D. Ligun, Nucl. Instrum. Methods Phys. Res. A **365**, 291 (1995).
[5] N. Faure, C. Borel, M. Couchaud, G. Basset, R. Templier, and C. Wyon, Appl. Phys. B **63**, 593 (1996).
[6] M. Itoh and T. Sakurai, Phys. Rev. B **73**, 235106 (2006).
[7] A. N. Belsky, V. V. Mikhailin, A. N. Vasil'ev, I. Dafinei, P. Lecoq, C. Pedrini, P. Chevallier, P. Dhez, and P. Martin, Chem. Phys. Lett. **243**, 552 (1995).
[8] Y. X. Fan, Y. Liu, Y. H. Duan, Q. Wang, L. Fan, H. T. Wang, G. H. Jia, and C. Y. Tu, Appl. Phys. B **93**, 327 (2008).
[9] F. A. Danevich, A. Sh. Georgadze, V. V. Kobychev, B. N. Kropivyansky, S. S. Nagorny, A. S. Nikolaiko, D. V. Poda, V. I. Tretyak, I. M. Vyshnevskyi, S. S. Yurchenko, B. V. Grinyov, L. L. Nagornaya, E. N. Pirogov, V. D. Ryzhikov, V. B. Brudanin, Ts. Vylov, A. Fedorov, M. Korzhik, A. Lobko, and O. Missevitch, Nucl. Instrum. Methods Phys. Res. A **556**, 259 (2006).
[10] R. M. Hazen, L. W. Finger, and J. W. E. Mariathasan, J. Phys. Chem. Solids **46**, 253 (1985).
[11] V. Panchal, N. Garg, A. K. Chauhan, Sangeeta, and S. M. Sharma, Solid State Commun. **130**, 203 (2004).
[12] D. Errandonea, Phys. Status Solidi B **242**, 125 (2005).
[13] J. Ruiz-Fuertes, D. Errandonea, O. Gomis, A. Friedrich, and F. J. Manjón, J. Appl. Phys. **115**, 043510 (2014).
[14] J. Ruiz-Fuertes, D. Errandonea, S. López-Moreno, J. González, O. Gomis, R. Vilaplana, F. J. Manjón, A. Muñoz, P. Rodríguez-Hernández, A. Friedrich, I. A. Tupitsyna, and L. L. Nagornaya, Phys. Rev. B **83**, 214112 (2011).
[15] R. Mittal, A. B. Garg, V. Vijayakumar, S. N. Achary, A. K. Tyagi, B. K. Godwal, E. Busetto, A. Lausi, and S. L. Chaplot, J. Phys.: Condens. Matter **20**, 075223 (2008).
[16] E. Bandiello, D. Errandonea, D. Martinez-Garcia, D. Santamaria-Perez, and F. J. Manjón, Phys. Rev. B **85**, 024108 (2012).
[17] D. Errandonea, J. Pellicer-Porres, F. J. Manjón, A. Segura, Ch. Ferrer-Roca, R. S. Kumar, O. Tschauner, P. Rodríguez-Hernández, J. López-Solano, S. Radescu, A. Mujica, A. Muñoz, and G. Aquilanti, Phys. Rev. B **72**, 174106 (2005).
[18] D. Errandonea, R. S. Kumar, X. Ma, and C. Tu, J. Solid State Chem. **181**, 355 (2008).
[19] D. Errandonea, J. Pellicer-Porres, F. J. Manjón, A. Segura, Ch. Ferrer-Roca, R. S. Kumar, O. Tschauner, J. López-Solano, P. Rodríguez-Hernández, S. Radescu, A. Mujica, A. Muñoz, and G. Aquilanti, Phys. Rev. B **73**, 224103 (2006).
[20] D. Errandonea, M. Somayazulu, and D. Häusermann, Phys. Status Solidi B **235**, 162 (2003).
[21] D. Errandonea, S. N. Achary, J. Pellicer-Porres, and A. K. Tyagi, Inorg. Chem. **52**, 5464 (2013).
[22] X. Wang, I. Loa, K. Syassen, M. Hanfland, and B. Ferrand, Phys. Rev. B **70**, 064109 (2004).
[23] D. Errandonea, R. Lacomba-Perales, J. Ruiz-Fuertes, A. Segura, S. N. Achary, and A. K. Tyagi, Phys. Rev. B **79**, 184104 (2009).
[24] O. Fukunaga and S. Yamaoka, Phys. Chem. Miner. **5**, 167 (1979).
[25] J. López-Solano, P. Rodríguez-Hernández, S. Radescu, A. Mujica, A. Muñoz, D. Errandonea, F. J. Manjón, J. Pellicer-Porres, N. Garro, A. Segura, Ch. Ferrer-Roca, R. S. Kumar, O. Tschauner, and G. Aquilanti, Phys. Status Solidi B **244**, 325 (2007).

[26] F. J. Manjón, D. Errandonea, J. López-Solano, P. Rodríguez-Hernández, S. Radescu, A. Mujica, A. Muñoz, N. Garro, J. Pellicer-Porres, A. Segura, Ch. Ferrer-Roca, R. S. Kumar, O. Tschauner, and G. Aquilanti, Phys. Status Solidi B **244**, 295 (2007).
[27] J. Ruiz-Fuertes, S. López-Moreno, D. Errandonea, J. Pellicer-Porres, R. Lacomba-Perales, A. Segura, P. Rodríguez-Hernández, A. Muñoz, A. H. Romero, and J. González, J. Appl. Phys. **107**, 083506 (2010).
[28] O. Gomis, J. A. Sans, R. Lacomba-Perales, D. Errandonea, Y. Meng, J. C. Chervin, and A. Polian, Phys. Rev. B **86**, 054121 (2012).
[29] R. Vilaplana, R. Lacomba-Perales, O. Gomis, D. Errandonea, and Y. Meng, Solid State Sci. **36**, 16 (2014).
[30] Y. Liu, S. Qin, J. Wu, X. Li, Y. Li, and J. Liu, Chin. Phys. C **33**, 1023 (2009).
[31] D. Errandonea, D. Santamaria-Perez, V. Grover, S. N. Achary, and A. K. Tyagi, J. Appl. Phys. **108**, 073518 (2010).
[32] R. Vilaplana, O. Gomis, F. J. Manjón, P. Rodríguez-Hernández, A. Muñoz, D. Errandonea, S. N. Achary, and A. K. Tyagi, J. Appl. Phys. **112**, 103510 (2012).
[33] Y. Fei, A. Ricolleau, M. Frank, K. Mibe, G. Shen, and V. Prakapenka, Proc. Natl. Acad. Sci. USA **104**, 9182 (2007).
[34] M. Yokoo, N. Kawai, K. G. Nakamura, K. Kondo, Y. Tange, and T. Tsuchiya, Phys. Rev. B **80**, 104114 (2009).
[35] J. Liu, L. Dubrovinsky, T. B. Ballaran, and W. Crichton, High Press. Res. **27**, 483 (2007).
[36] L. Dubrovinsky, K. Glazyrin, C. McCammon, O. Narygina, E. Greenberg, S. Übelhack, A. I. Chumakov, S. Pascarelli, V. Prakapenka, J. Bock, and N. Dubrovinskaia, J. Synchrotron Radiat. **16**, 737 (2009).
[37] A. P. Hammersley, S. O. Svensson, M. Hanfland, A. N. Fitch, and D. Hausermann, High Press. Res. **14**, 235 (1996).
[38] B. H. Toby, J. Appl. Crystallogr. **34**, 210 (2001).
[39] D. Errandonea, Y. Meng, M. Somayazulu, and D. Häusermann, Physica B **355**, 116 (2005).
[40] S. Klotz, J-C. Chervin, P. Munsch, and G. L. Marchand, J. Phys. D, Appl. Phys. **42**, 075413 (2009).
[41] P. Botella, R. Lacomba-Perales, D. Errandonea, A. Polian, P. Rodríguez-Hernández, and A. Muñoz, Inorg. Chem. **53**, 9729 (2014).
[42] U. Häussermann, P. Berastegui, S. Carlson, J. Haines, and J. Léger, Angew. Chem. **113**, 4760 (2001).
[43] A. Grzechnik, W. A. Crichton, and M. Hanfland, Phys. Status Solidi B **242**, 2795 (2005).
[44] D. Liu, W. W. Lei, J. Hao, D. D. Liu, B. B. Liu, X. Wang, X. H. Chen, Q. L. Cui, G. T. Zou, J. Liu, and S. Jiang, J. Appl. Phys. **105**, 023513 (2009).
[45] M. Pravica, L. Bai, D. Sneed, and C. Park, J. Phys. Chem. A **117**, 2302 (2013).
[46] A. B. Garg, D. Errandonea, P. Rodríguez-Hernández, S. López-Moreno, A. Muñoz, and C. Popescu, J. Phys.: Condens. Matter **26**, 265402 (2014).
[47] D. Errandonea, F. J. Manjón, M. Somayazulu, and D. Häusermann, J. Solid State Chem. **177**, 1087 (2004).
[48] F. Birch, Phys. Rev. **71**, 809 (1947).
[49] R. Lacomba-Perales, D. Martínez-García, D. Errandonea, Y. L. Godec, J. Philippe, and G. Morard, High Press. Res. **29**, 76 (2009).
[50] R. Lacomba-Perales, D. Martinez-García, D. Errandonea, Y. L. Godec, J. Philippe, G. L. Marchand, J. C. Chervin, A. Polian, A. Múñoz, and J. López-Solano, Phys. Rev. B **81**, 144117 (2010).
[51] D. Errandonea and F. J. Manjón, Prog. Mater. Sci. **53**, 711 (2008).